Metalloporphyrin Mixed-Valence π-Cation Radicals: Solid-State Structures

W. Robert Scheidt,* Kristin E. Brancato-Buentello, Hungsun Song, K. Venugopal Reddy, and Beisong Cheng

Department of Chemistry and Biochemistry, University of Notre Dame, Notre Dame, Indiana 46556

Received September 6, 1996[⊗]

The synthesis and structural characterization of three mixed-valence π-cation radical derivatives of (octaethylporphinato)metal(II) species, $[M(OEP^{\bullet/2})]_2^+$, (M = Ni, Cu, and (Zn,H_2)), are reported. The species thus have the same formal ring oxidation level as the photooxidized special pair of photosynthetic reaction centers. The complexes display unique binuclear structures with cofacial porphyrin rings with mean plane separations of 3.20−3.32 Å, ring center to ring center distances of 3.50−3.55 Å, and lateral shifts between the two rings of 1.16−1.53 Å. These inter-ring geometries are distinctly different from either those of "classical" π-cation radical derivatives or those of dimers formed by neutral species. The different inter-ring geometries suggests that there are inherent inter-ring geometries that depend principally on the oxidation level of the porphyrin rings.

Introduction

Electronic interactions between the π-systems of two or more porphyrin molecules in close proximity are believed to be important in defining the properties of the supramolecular ensemble. Notable examples of such interacting porphyrin π systems are those found in photosynthetic proteins[1] and in linearly stacked arrays that are organic conductors.[2] The photosynthetic proteins include the light-harvesting chlorophyll arrays[3] and the photosynthetic reaction center (RC)[4] special pairs.[5] The photoinduced formation of the one electron oxidized reaction center special pair (the primary donor, often called P^+) is the first step in the conversion of light energy to chemical energy. The special pair of the reaction center from the purple bacterium *Rhodopseudomonas viridis* has two bacteriochlorophyll planes separated by about 3.3 Å in a "slipped" conformation, as shown by an X-ray structure determination.[6] Structures of reaction centers from other bacteria show similar structures for their special pairs.[7] The special pair has important physicochemical properties, and an understanding of the structural basis for the interaction of the pair of bacteriochlorophylls is of interest.

As part of our studies examining ring−ring interactions in porphyrin derivatives, we have been investigating the solid-state structures of π-cation radical derivatives with minimal steric encumbrance at the molecular periphery. In 1989 we presented the first octaethylporphyrin π-cation radical crystal structure, that of the compound $[Zn(OEP^{\bullet})(OH_2)]ClO_4$.[4,8] Significant and novel features that were first observed in this zinc derivative have also been seen in other members of this class of π-cation radicals.[9−11] These π-cation radical derivatives all form cofacial dimers with relatively small interplanar spacings between the two porphyrin planes. Furthermore, the two porphyrin rings are completely overlapped. The degree of ring−ring overlap is completely different from that exhibited by interacting neutral (unoxidized) porphyrin ring derivatives which form cofacial dimers with much weaker (smaller) ring−ring overlaps. Despite the weaker interactions, there are still only a limited number of characteristic geometries observed for the members of this porphyrin ring oxidation class.[12]

In this paper, we describe the synthesis and structural characterization of three examples of a novel class of π-cation radical metalloporphyrin derivatives. In these derivatives metallooctaethylporphyrins have been oxidized by one electron equivalent per two porphyrin rings to form the species $[M(OEP^{\bullet/2})]_2^+$, which possess a single electron hole per *pair* of porphyrin rings. The species thus have the same formal ring oxidation level as the photooxidized special pair of reaction centers. In all derivatives, the two rings are crystallographically equivalent, which is consistent with the one electron being delocalized over two macrocycles. We have suggested "mixed-valence π-cation radical" as a descriptive name for this new class of synthetic porphyrin derivatives. The species that have been crystallographically characterized are two homobinuclear derivatives, $[Ni(OEP^{\bullet/2})]_2SbCl_6$, and $[Cu(OEP^{\bullet/2})]_2SbCl_6$, and a heterobinuclear derivative with idealized formula $[Zn(OEP^{\bullet/2})H_2(OEP^{\bullet/2})]SbCl_6$.

The structure determinations show that these mixed-valence π-cation radicals form cofacial, dimeric, supramolecular as-

[⊗] Abstract published in *Advance ACS Abstracts,* November 15, 1996.

(1) (a) Gregory, R. P. F. *Photosynthesis*; Chapman and Hall: New York, 1989. (b) *Photosynthesis*; Amesz, J., Ed.; Elsevier: New York, 1987.
(2) Hoffman, B. M.; Ibers, J. A. *Acc. Chem. Res.* **1983**, *16*, 15.
(3) (a) Kühlbrandt, W.; Wang, D. N.; Fujiyoshi, Y. *Nature (London)* **1994**, *367*, 614. (b) McDermott, G.; Prince, S. M.; Freer, A. A.; Hawthornthwaite-Lawless, A. M.; Papiz, M. Z.; Cogdell, R. J.; Isaacs, N. W. *Nature (London)* **1995**, *374*, 517.
(4) Abbreviations used in this paper: RC, photosynthetic reaction center; P, the bacteriochlorophyll special pair; OEP, octaethylporphyrin; $OEP^{\bullet}$, octaethylporphyrin π-cation radical; $OEP^{\bullet/2}$, octaethylporphyrin mixed-valence π-cation radical; Ct, center of the 24-atom porphyrin ring; N_p, pyrrole nitrogen; MPS, mean plane separation; LS, lateral shift.
(5) *The Photosynthetic Reaction Center*; Deisenhofer, J., Norris, J. R., Eds.; Academic Press: New York, 1993; Vol. 2.
(6) (a) Deisenhofer, J.; Epp, O.; Miki, K.; Huber, R.; Michel, H. *J. Mol. Biol.* **1984**, *180*, 385. (b) Deisenhofer, J.; Epp, O.; Miki, K.; Huber, R.; Michel, H. *Nature (London)* **1985**, *318*, 618. (c) Deisenhofer, J.; Epp, O.; Sinning, I.; Michel, H. *J. Mol. Biol.* **1995**, *246*, 429.
(7) (a) Allen, J. P.; Feher, G. *Proc. Natl. Acad. Sci. U.S.A.* **1984**, *81*, 4795. (b) Chang, C.-H., Tiede, D.; Tang, J.; Smith, U.; Norris, J.; Schiffer, M. *FEBS* **1986**, *205*, 3951. (c) El-Kabbani, O.; Chang, C.-H.; Tiede, D.; Norris, J.; Schiffer, M. *Biochemistry* **1991**, *30*, 5361. (d) Chirona, A. J.; Lous, E. J.; Huber, M.; Allen, J. P.; Schenck, C.; Paddock, M. L.; Feher, G.; Rees, D. C. *Biochemistry* **1994**, *33*, 4584. (e) Ermler, U.; Fritzsch, G.; Buchanan, S.; Michel, H. *Structure* **1994**, *2*, 925.
(8) Song, H.; Reed, C. A.; Scheidt, W. R. *J. Am. Chem. Soc.* **1989**, *111*, 6867.
(9) Brancato-Buentello, K. E.; Reddy K. V.; Cheng, B.; Scheidt, W. R. Manuscript in progress.
(10) Scheidt, W. R.; Song, H.; Haller, K. J.; Safo, M. K.; Orosz, R. D.; Reed, C. A.; Debrunner, P. G.; Schulz, C. E. *Inorg. Chem.* **1992**, *31*, 939.
(11) Song, H.; Orosz, R. D.; Reed, C. A.; Scheidt, W. R. *Inorg. Chem.* **1990**, *29*, 4274.
(12) Scheidt, W. R.; Lee, Y. J. *Struc. Bonding (Berlin)* **1987**, *64*, 1.

S0020-1669(96)01074-9 CCC: $12.00

Table 1. Crystallographic details for $[Ni(OEP^{\bullet/2})]_2SbCl_6$, $[Cu(OEP^{\bullet/2})]_2SbCl_6$, and $[Zn(OEP^{\bullet/2})H_2(OEP^{\bullet/2})]SbCl_6$

formula	$C_{72}H_{88}SbNi_2Cl_6N_8.CH_2Cl_2$	$C_{72}H_{88}SbCu_2Cl_6N_8.^1/_2CH_2Cl_2.^1/_2CHCl_3$	$C_{72}H_{90}SbZnCl_6N_8.^1/_3CH_2Cl_2.^2/_3CHCl3$
FW, amu	1602.38	1556.01	1684.50
a, Å	16.744(6)	14.791(3)	14.744(4)
b, Å	14.785(2)	17.042(5)	17.156(9)
c, Å	29.173(5)	14.796(3)	14.887(6)
β, deg	90.0	99.87 (2)	99.95(10)
V, Å^3	7221.9	3674.4	3709.0
space group	*Pbcn*	$P2_1/c$	$P2_1/a$
Z	4	2	2
temp, K	124 ± 2	125 ± 2	127 ± 2
λ, Å	0.710 73	0.710 73	0.710 73
D_c, g/cm^3	1.47	1.41	1.51
μ, mm^{-1}	1.238	1.278	1.411
diffractometer	CAD4	CAD4	FAST
no. of data used in refinement	3960[a]	5623[a]	9782[b]
final *R* indices	R_1[c] = 0.073; R_2[d] = 0.075	R_1[c] = 0.072; R_2[d] = 0.077	R_1[c] = 0.077; wR_2[e] = 0.1919; for all data

[a] Observed data $F_o \geq 3\sigma(F_o)$. [b] Total unique data including negative F^2, 5687 "observed" data with $F^2 > 2\sigma(F^2)$, all 9782 data used in least-squares refinement. [c] $R_1 = \Sigma||F_o| - |F_c||/\Sigma|F_o|$. [d] $R_2 = [\Sigma w(|F_o| - |F_c|)^2/\Sigma w(F_o)_2]^{1/2}$. [e] $[\Sigma[w(F_o^2 - F_c^2)^2]/\Sigma[w(F_o^2)^2]]^{1/2}$.

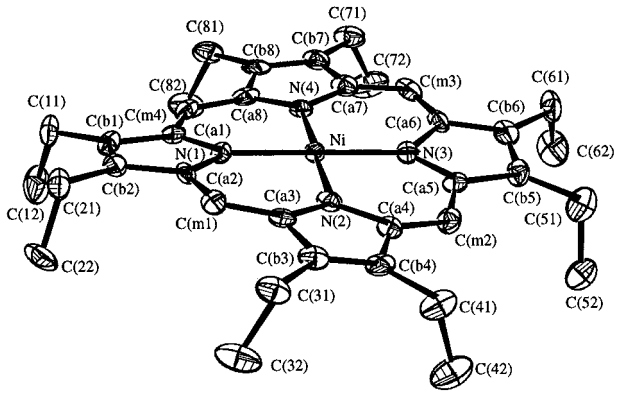

Figure 1. ORTEP drawing of the crystallographically independent portion of the $[Ni(OEP^{\bullet/2})]_2^+$ mixed-valence π-cation radical showing the atom numbering scheme. Thermal ellipsoids are drawn to illustrate 50% probability surfaces.

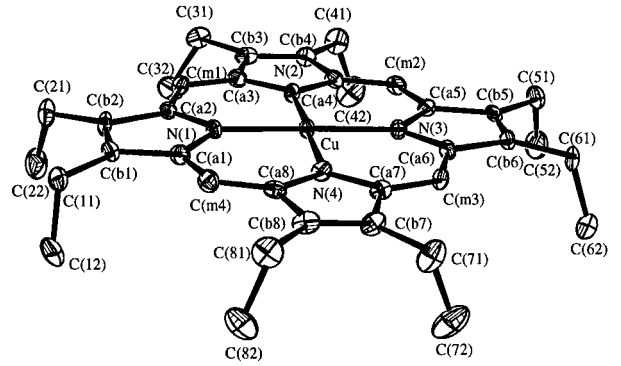

Figure 2. ORTEP drawing of the crystallographically independent portion of the $[Cu(OEP^{\bullet/2})]_2^+$ mixed-valence π-cation radical showing the atom numbering scheme. Thermal ellipsoids are drawn to illustrate 50% probability surfaces.

semblies. Again this particular class has very similar porphyrin ring to ring geometries. However, the geometry of the ring−ring interactions in these cofacial dimers is distinctly different from either those of "classical" π-cation radical derivatives or those formed by neutral porphyrins. The essential similarity in ring−ring interactions within each class and the significant differences in ring−ring geometry between the various classes suggests that there are inherent proximity geometries that depend principally on the oxidation level of the porphyrin rings.

Experimental Section

General Information. Dichloromethane, chloroform, and hexane were purchased from Fisher, H_2OEP from Midcentury Chemicals, and tris(4-bromophenyl)aminium hexachloroantimonate from Aldrich. Dichloromethane and chloroform were distilled from CaH_2 and hexane from sodium/benzophenone under argon. All reactions were performed under an argon atmosphere with oven-dried Schlenkware and cannula techniques. Metals were inserted into free-base H_2OEP by standard methods.[13] IR spectra were recorded on a Perkin-Elmer 883 infrared spectrophotometer as KBr pellets, and absorption spectra were recorded on a Perkin-Elmer Lambda 19 UV/vis/near-IR spectrometer.

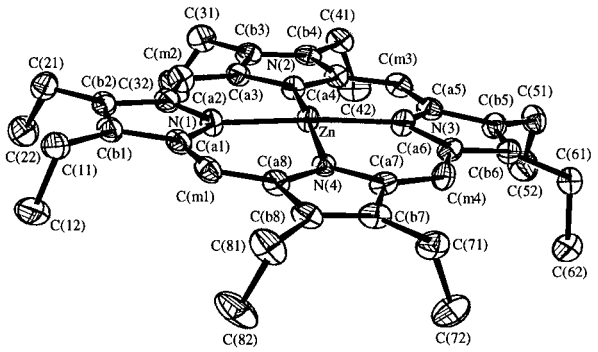

Figure 3. ORTEP diagram with atom-labeling scheme for the $[Zn(OEP^{\bullet/2})H_2(OEP^{\bullet/2})]^+$ mixed-valence π-cation radical. Thermal ellipsoids are drawn at the 50% probability level. Porphyrin hydrogen atoms are omitted for clarity.

Syntheses. $[Ni(OEP^{\bullet/2})]_2SbCl_6\cdot CH_2Cl_2$. Ni(OEP) (55 mg, 0.093 mmol) and tris(4-bromophenyl)aminium hexachloroantimonate (40 mg, 0.049 mmol) were placed in a 100-mL Schlenk flask. Dichloromethane (~12 mL) was added through a cannula, and the solution was stirred for 1 h. The solution was then evenly transferred from the Schlenk reaction flask into two 10-mL beakers which were each placed in a crystallizing bottle with CH_2Cl_2:hexane (1:1) to induce crystallization by slow vapor diffusion. Dark purple single crystals formed after ~5 days; an X-ray analysis confirmed that the compound was $[Ni(OEP^{\bullet/2})]_2SbCl_6\cdot CH_2Cl_2$. UV/vis/near-IR ($CH_2Cl_2$): λ_{max} 392 (Soret), 516, 552, 1540 nm. IR (KBr): ν (OEP$^\bullet$) 1570 cm^{-1} (strong).

$[Cu(OEP^{\bullet/2})]_2SbCl_6\cdot{}^1/_2CH_2Cl_2\cdot{}^1/_2CHCl_3$. Cu(OEP) (60 mg, 0.101 mmol) in ~12 mL of CH_2Cl_2 and 4 mL of $CHCl_3$ was reacted with tris(4-bromophenyl)aminium hexachloroantimonate (44 mg, 0.054 mmol) in a 100-mL Schlenk flask. After about 1 h, the solution was filtered into beakers kept in crystallizing bottles with CH_2Cl_2:hexane (1:1). After ~4 days, brown-violet X-ray quality crystals were obtained. UV/vis/near-IR (CH_2Cl_2): λ_{max} 396 (Soret), 525, 562, 1541 nm. IR (KBr): ν (OEP$^\bullet$) 1548 cm^{-1} (strong).

$[Zn(OEP^{\bullet/2})H_2(OEP^{\bullet/2})]SbCl_6\cdot{}^1/_3CH_2Cl_2\cdot{}^2/_3CHCl_3$. $[Zn(OEP^{\bullet/2})H_2(OEP^{\bullet/2})]SbCl_6$ was obtained by reacting Zn(OEP) (60 mg, 0.101 mmol) and tris(4-bromophenyl)aminium hexachloroantimonate (44 mg, 0.054 mmol) in ~50 mL of CH_2Cl_2 in a 100-mL Schlenk flask. After

(13) Adler, A. D.; Longo, F. R.; Kampas, F.; Kim, J. *J. Inorg. Nucl. Chem.* **1970**, *32*, 2443.

Table 2. Bond Lengths for $[Ni(OEP^{\bullet/2})]_2SbCl_6 \cdot CH_2Cl_2$, $[Cu(OEP^{\bullet/2})]_2SbCl_6 \cdot {}^1/_2CH_2Cl_2 \cdot {}^1/_2CHCl_3$, and $[Zn(OEP^{\bullet/2})H_2(OEP^{\bullet/2})]SbCl_6 \cdot {}^1/_3CH_2Cl_2 \cdot {}^2/_3CHCl_3$[a]

	length (Å)				length (Å)		
	M = Ni	M = Cu	M = Zn,H_2		M = Ni	M = Cu	M = Zn,H_2
M−N(1)	1.940(5)	1.991(3)	2.041(4)	C(b1)−C(b2)	1.332(11)	1.347(5)	1.365(7)
M−N(2)	1.956(6)	1.983(3)	2.064(4)	C(b3)−C(b4)	1.333(11)	1.362(5)	1.353(6)
M−N(3)	1.952(5)	1.977(3)	2.043(4)	C(b5)−C(b6)	1.351(12)	1.357(6)	1.357(6)
M−N(4)	1.951(5)	1.986(3)	2.064(4)	C(b7)−C(b8)	1.338(11)	1.353(5)	1.354(7)
N(1)−C(a1)	1.386(9)	1.381(5)	1.370(5)	C(b1)−C(11)	1.503(10)	1.495(6)	1.500(6)
N(1)−C(a2)	1.383(8)	1.376(5)	1.369(6)	C(b2)−C(21)	1.505(10)	1.491(5)	1.496(7)
N(2)−C(a3)	1.380(9)	1.376(5)	1.365(6)	C(b3)−C(31)	1.501(10)	1.494(5)	1.492(7)
N(2)−C(a4)	1.377(9)	1.362(5)	1.367(5)	C(b4)−C(41)	1.515(11)	1.496(5)	1.502(6)
N(3)−C(a5)	1.342(9)	1.394(5)	1.368(5)	C(b5)−C(51)	1.503(11)	1.482(6)	1.500(6)
N(3)−C(a6)	1.397(9)	1.375(5)	1.369(6)	C(b6)−C(61)	1.523(11)	1.500(5)	1.490(7)
N(4)−C(a7)	1.365(9)	1.369(5)	1.355(6)	C(b7)−C(71)	1.498(11)	1.507(6)	1.500(7)
N(4)−C(a8)	1.370(10)	1.373(5)	1.369(5)	C(b8)−C(81)	1.474(12)	1.502(6)	1.490(6)
C(a1)−C(b1)	1.437(10)	1.460(5)	1.443(6)	C(11)−C(12)	1.500(13)	1.523(6)	1.508(7)
C(a2)−C(b2)	1.447(9)	1.455(5)	1.442(6)	C(21)−C(22)	1.518(12)	1.531(6)	1.518(8)
C(a3)−C(b3)	1.449(10)	1.448(5)	1.453(6)	C(31)−C(32)	1.532(12)	1.519(6)	1.516(8)
C(a4)−C(b4)	1.464(12)	1.457(5)	1.445(6)	C(41)−C(42)	1.541(12)	1.516(7)	1.517(7)
C(a5)−C(b5)	1.471(10)	1.460(5)	1.443(6)	C(51)−C(52)	1.570(13)	1.528(6)	1.526(7)
C(a6)−C(b6)	1.444(10)	1.455(5)	1.459(6)	C(61)−C(62)	1.533(12)	1.518(6)	1.526(8)
C(a7)−C(b7)	1.457(12)	1.449(5)	1.450(6)	C(71)−C(72)	1.522(13)	1.507(7)	1.512(8)
C(a8)−C(b8)	1.460(11)	1.456(5)	1.451(6)	C(81)−C(82)	1.525(12)	1.522(7)	1.520(8)
C(a1)−C(m4)	1.368(11)	1.368(5)	1.384(7)	Sb−Cl(1)	2.328(4)	2.290(3)	2.359(4)
C(a2)−C(m1)	1.364(10)	1.361(6)	1.397(6)	Sb−Cl(2)	2.316(5)	2.429(2)	2.406(9)
C(a3)−C(m1)	1.375(10)	1.382(5)	1.390(6)	Sb−Cl(3)	2.380(7)	2.355(3)	2.334(5)
C(a4)−C(m2)	1.360(11)	1.385(5)	1.392(6)	Sb−Cl(4)	2.349(6)	2.369(3)	2.304(8)
C(a5)−C(m2)	1.372(11)	1.368(5)	1.391(6)	Sb−Cl(5)	2.338(6)	2.331(3)	2.372(3)
C(a6)−C(m3)	1.345(11)	1.377(6)	1.390(6)	Sb−Cl(6)	2.349(3)	2.352(3)	2.351(4)
C(a7)−C(m3)	1.399(11)	1.392(5)	1.400(6)	C−Cl(7)	1.768(4)	1.80(1)	1.771(16)
C(a8)−C(m4)	1.389(11)	1.366(5)	1.396(6)	C−Cl(8)	1.767(4)	1.72(1)	1.730(14)
				C−Cl(9)		1.68(1)	1.681(16)

[a] The estimated standard deviations of the least significant digits are given in parentheses.

1 h of stirring, the volume was reduced to ~15 mL. The solution was then transferred from the Schlenk reaction flask into a 50-mL Schlenk flask by a cannula and then layered with hexane for crystallization. The dark purple crystals that formed after ~4 days were subjected to an X-ray structure analysis that showed the material had partially demetalated. The idealized formula of the compound is $[Zn(OEP^{\bullet/2})H_2(OEP^{\bullet/2})]SbCl_6$. The spectroscopic properties of the compound were obtained from mixing experiments as described elsewhere.[14] UV/vis/near-IR (CH_2Cl_2): λ_{max} 396(Soret), 499, 531, 553 (sh), 565, 599, 619, 672, 930 nm.

X-ray Structure Determinations. $[Ni(OEP^{\bullet/2})]_2SbCl_6$ and $[Cu(OEP^{\bullet/2})]_2SbCl_6$. A brown $[Ni(OEP^{\bullet/2})]_2SbCl_6$ fragment and a brown-violet, truncated hexagonal bipyramidal single crystal of $[Cu(OEP^{\bullet/2})]_2SbCl_6$ were mounted on hollow glass fibers with their plates normal approximately parallel to the goniometer head axis. Cell constants were obtained from least-squares refinement of 25 automatically centered reflections. A brief summary of crystal data and data collection parameters for $[Ni(OEP^{\bullet/2})]_2SbCl_6$ and $[Cu(OEP^{\bullet/2})]_2SbCl_6$ is listed in Table 1; complete crystallographic details are included in the Supporting Information. As a check on crystal quality, ω-scans of several intense reflections were measured; the average width at half-height for $[Ni(OEP^{\bullet/2})]_2SbCl_6$ was 0.32° with a take-off angle of 2.8° indicating fair crystal quality and that of $[Cu(OEP^{\bullet/2})]_2SbCl_6$ was 0.20° with the same take-off angle indicating good crystal quality. Lorentz and polarization factors were applied to the data as well as an empirical absorption correction. The $[Ni(OEP^{\bullet/2})]_2SbCl_6$ structure was solved by direct methods (MULTAN).[15] The antimony atom was found in a general position at half occupancy and thus disordered over two sites. Hydrogen atoms were included as idealized riding model contributors with their thermal parameters determined by the respective carbon atoms to which they were attached. The structure of $[Cu(OEP^{\bullet/2})]_2SbCl_6$ was solved by Patterson methods which provided coordinates for the half-antimony atom and the copper atom. Difference Fourier maps revealed positions for the remaining atoms of the metalloporphyrin and the hexachloroantimonate as well as the positions for a disordered solvent. The solvent region was described as a mixed chloroform and methylene chloride molecule site; the presence of both molecules in the crystals was confirmed by mass spectrometry. Full-matrix least-squares refinements utilized observed data with $F_o \geq 3.0\sigma(F_o)$, and led to the discrepancy indices in Table 1. The model for the final cycles of refinement assigned porphyrinate hydrogen atoms as idealized isotropic fixed contributors. The disordered solvent hydrogens were not included in the calculation. Atomic coordinates for the structures are presented in Tables S2 and S6, respectively, while complete crystallographic details can be found in Tables S1 and S5. Anisotropic thermal parameters and the fixed hydrogen atom coordinates for both structures are included in the Supporting Information.

$[Zn(OEP)H_2(OEP^{\bullet/2})]SbCl_6$. A platelike, violet crystal of $[Zn(OEP^{\bullet/2})H_2(OEP^{\bullet/2})]SbCl_6$ was mounted on the end of a hollow glass fiber. X-ray diffraction data were collected on an Enraf-Nonius FAST area detector with a Mo rotating anode source (λ = 0.710 73 Å) at 127 ± 2 K. Our detailed methods and procedures for small molecule X-ray data collection with the FAST system have been described previously.[16] Preliminary examination of the crystal established a two-molecule monoclinic unit cell, space group $P2_1/a$. Data were corrected for Lorentz and polarization factors and absorption effects. The

(14) Brancato-Buentello, K. E.; Kang, S.-J.; Scheidt, W. R. Submitted for publication.

(15) (a) Direct Methods Program MULTAN: Main, P.; Hull, S. E.; Lessinger, L.; Germain, G.; Declercq, J. P.; Woolfson, M. M. MULTAN, a system of computer programs for the automatic solution of crystal structures from X-ray diffraction data. University of York, York, England, 1982. (b) Local modified least-square refinement: Lapp, R. L.; Jacobson, R. A. ALLS, a generalized crystallographic least-squares program, National Technical Information Services IS-4708 UC-4, Springfield, VA. (c) Busing and Levy's ORFFE and ORFLS and Johnson's ORTEP2. (d) Atomic form factors were from the following: Cromer, D. T.; Mann, J. B. *Acta Crystallogr., Sect. A* **1968**, *24*, 321. Real and imaginary corrections for anomalous dispersion in the form factor of the nickel and copper atoms were from the following: Cromer, D. T.; Liberman, D. J. *J. Chem. Phys.* **1970**, *53*, 1891. Scattering factors for hydrogen were from the following: Stewart, R. F.; Davidson, E. R.; Simpson, W. T. *Ibid.* **1965**, *42*, 3175.

(16) Scheidt, W. R.; Turowska-Tyrk, I. *Inorg. Chem.* **1994**, *33*, 1314.

Table 3. Bond angles for $[Ni(OEP^{\bullet/2})]_2SbCl_6\cdot CH_2Cl_2$, $[Cu(OEP^{\bullet/2})]_2SbCl_6\cdot{}^1/_2CH_2Cl_2\cdot{}^1/_2CHCl_3$, and $[Zn(OEP^{\bullet/2})H_2(OEP^{\bullet/2})]SbCl_6\cdot{}^1/_3CH_2Cl_2\cdot{}^2/_3CHCl_3$[a]

	angle (deg)				angle (deg)		
	M = Ni	M = Cu	M = Zn,H_2		M = Ni	M = Cu	M = Zn,H_2
N(1)−M−N(2)	89.6(2)	89.8(1)	90.14(15)	C(m3)−C(a6)−C(b6)	124.0(7)	124.5(4)	123.8(4)
N(1)−M−N(3)	179.3(3)	178.8(1)	174.7(2)	C(m3)−C(a7)−C(b7)	123.7(7)	123.9(4)	125.4(4)
N(1)−M−N(4)	90.6(2)	89.8(1)	90.21(14)	C(m4)−C(a8)−C(b8)	124.1(7)	124.4(4)	125.7(4)
N(2)−M−N(3)	89.9(3)	90.3(1)	89.42(14)	C(b2)−C(b1)−C(a1)	106.4(6)	106.7(3)	107.1(4)
N(2)−M−N(4)	178.1(2)	177.1(1)	171.4(2)	C(b1)−C(b2)−C(a2)	108.0(6)	106.9(3)	106.6(4)
N(3)−M−N(4)	89.8(3)	90.0(1)	89.44(14)	C(b4)−C(b3)−C(a3)	107.2(7)	106.9(3)	107.2(4)
C(a1)−N(1)−M	127.5(4)	127.3(3)	126.3(3)	C(b3)−C(b4)−C(a4)	107.1(7)	106.6(3)	106.9(4)
C(a2)−N(1)−M	128.3(4)	127.3(3)	126.3(3)	C(b6)−C(b5)−C(a5)	106.5(7)	105.9(3)	106.9(4)
C(a3)−N(2)−M	127.6(5)	127.7(3)	125.8(3)	C(b5)−C(b6)−C(a6)	106.1(7)	107.2(3)	106.3(4)
C(a4)−N(2)−M	127.0(5)	127.1(2)	126.8(3)	C(b8)−C(b7)−C(a7)	106.2(7)	106.4(3)	107.0(4)
C(a5)−N(3)−M	127.5(5)	127.3(3)	126.9(3)	C(b7)−C(b8)−C(a8)	106.4(7)	106.7(3)	106.7(4)
C(a6)−N(3)−M	127.6(5)	128.1(3)	126.3(3)	C(a1)−C(b1)−C(11)	123.4(7)	123.8(4)	124.2(4)
C(a7)−N(4)−M	128.3(5)	127.4(3)	127.1(3)	C(a2)−C(b2)−C(21)	123.9(7)	124.2(4)	125.2(4)
C(a8)−N(4)−M	127.5(5)	127.3(3)	125.6(3)	C(a3)−C(b3)−C(31)	123.9(7)	124.5(4)	125.0(4)
C(a1)−N(1)−C(a2)	104.3(6)	105.1(3)	107.0(4)	C(a4)−C(b4)−C(41)	123.9(7)	125.4(3)	124.2(4)
C(a3)−N(2)−C(a4)	105.4(6)	105.3(3)	107.4(4)	C(a5)−C(b5)−C(51)	123.8(7)	125.2(4)	124.3(4)
C(a5)−N(3)−C(a6)	104.9(6)	104.5(3)	106.0(4)	C(a6)−C(b6)−C(61)	124.0(8)	124.5(4)	124.0(4)
C(a7)−N(4)−C(a8)	104.1(6)	105.3(3)	107.3(4)	C(a7)−C(b7)−C(71)	125.1(7)	124.1(4)	125.0(4)
N(1)−C(a1)−C(b1)	111.3(7)	110.6(3)	109.4(4)	C(a8)−C(b8)−C(81)	123.9(7)	124.5(4)	124.7(4)
N(1)−C(a2)−C(b2)	110.0(6)	110.8(4)	109.8(4)	C(b2)−C(b1)−C(11)	130.2(7)	129.4(4)	128.7(4)
N(2)−C(a4)−C(b4)	109.8(6)	110.9(3)	109.5(4)	C(b1)−C(b2)−C(21)	128.0(7)	128.8(4)	128.1(4)
N(2)−C(a3)−C(b3)	110.4(6)	111.3(3)	109.0(4)	C(b4)−C(b3)−C(31)	128.8(7)	129.6(4)	127.8(4)
N(3)−C(a5)−C(b5)	111.2(6)	111.2(3)	110.6(4)	C(b3)−C(b4)−C(41)	129.0(8)	127.9(4)	128.8(4)
N(3)−C(a6)−C(b6)	111.0(7)	111.2(3)	110.2(4)	C(b6)−C(b5)−C(51)	129.7(7)	128.9(4)	128.6(4)
N(4)−C(a7)−C(b7)	111.8(7)	111.2(3)	109.6(4)	C(b5)−C(b6)−C(61)	129.7(7)	128.2(4)	129.6(4)
N(4)−C(a8)−C(b8)	111.4(7)	110.5(3)	109.4(4)	C(b8)−C(b7)−C(71)	128.4(8)	129.5(4)	128.0(4)
N(1)−C(a1)−C(m4)	124.4(6)	124.4(4)	124.8(4)	C(b7)−C(b8)−C(81)	129.8(8)	128.7(4)	128.5(4)
N(1)−C(a2)−C(m1)	124.6(6)	124.7(3)	124.9(4)	C(a1)−C(m4)−C(a8)	124.8(7)	125.9(4)	127.6(4)
N(2)−C(a3)−C(m1)	125.1(7)	124.3(4)	125.3(4)	C(a2)−C(m1)−C(a3)	124.0(7)	126.0(4)	127.1(5)
N(2)−C(a4)−C(m2)	125.7(7)	125.6(3)	124.6(4)	C(a4)−C(m2)−C(a5)	122.9(7)	125.3(4)	127.0(4)
N(3)−C(a5)−C(m2)	126.6(7)	124.3(3)	125.0(4)	C(a6)−C(m3)−C(a7)	124.4(7)	125.1(4)	126.0(4)
N(3)−C(a6)−C(m3)	124.7(6)	124.3(3)	125.9(4)	C(b1)−C(11)−C(12)	110.7(7)	111.9(4)	112.4(4)
N(4)−C(a7)−C(m3)	124.4(7)	124.9(4)	124.9(4)	C(b2)−C(21)−C(22)	112.9(7)	112.5(4)	112.7(4)
N(4)−C(a8)−C(m4)	124.5(7)	125.1(4)	124.9(4)	C(b3)−C(31)−C(32)	111.6(7)	111.2(4)	113.6(5)
C(m4)−C(a1)−C(b1)	124.4(7)	125.0(4)	125.8(4)	C(b4)−C(41)−C(42)	111.2(7)	112.4(4)	113.0(4)
C(m1)−C(a2)−C(b2)	125.3(6)	124.5(4)	125.3(4)	C(b5)−C(51)−C(52)	109.4(8)	111.7(4)	113.0(4)
C(m1)−C(a3)−C(b3)	124.4(7)	124.4(4)	125.6(4)	C(b6)−C(61)−C(62)	110.5(7)	111.8(4)	112.7(4)
C(m2)−C(a4)−C(b4)	124.6(7)	123.5(4)	125.9(4)	C(b7)−C(71)−C(72)	113.1(7)	112.1(4)	113.1(4)
C(m2)−C(a5)−C(b5)	122.2(7)	124.5(4)	124.3(4)	C(b8)−C(81)−C(82)	112.9(7)	113.5(4)	112.9(5)

[a] The estimated standard deviations of the least significant digits are given in parentheses.

structure was refined by SHELXL-93.[17] The final refinement utilized porphyrinate hydrogen atoms as fixed isotropic contributors including the $CHCl_3$ solvent hydrogen atom. As in the $[Cu(OEP^{\bullet/2})]_2SbCl_6$ structure, this solvent region was described as a mixed chloroform and methylene chloride molecule site. At convergence, the final value for the unweighted *R* was 0.0773 for 5687 unique observed data and the weighted *R* (on F^2) was 0.1919 for 9782 unique measured data. Brief crystal data (including collection parameters) are given in Table 1, atomic coordinates are presented in Table S10, and the Supporting Information provides complete crystallographic data, anisotropic thermal parameters, and the fixed hydrogen atom coordinates.

Results

The molecular and crystal structures of three different mixed-valence π-cation radicals have been determined by X-ray analysis. The structure and labeling scheme of the unique portion of the $[Ni(OEP^{\bullet/2})]_2^+$ ion is shown in Figure 1. Figure 2 gives an ORTEP diagram for the crystallographically unique part of the $[Cu(OEP^{\bullet/2})]_2^+$ cation, which also illustrates the labeling scheme for all atoms used in the tables. An equivalent illustration for the heterobinuclear $[Zn(OEP^{\bullet/2})H_2(OEP^{\bullet/2})]^+$ ion is given in Figure 3.

The average Ni−N_p bond distance for the four-coordinate nickel ion in $[Ni(OEP^{\bullet/2})]_2^+$ is 1.950(7) Å; Tables 2 and 3 show values of distances and angles for all mixed-valence π-cation radicals. The four Cu−N_p bond distances for $[Cu(OEP^{\bullet/2})]_2^+$ have an average value of 1.984(6) Å. The average value of the Zn−N_p distance in $[Zn(OEP^{\bullet/2})H_2(OEP^{\bullet/2})]^+$ is 2.053(13) Å; the partial occupancy of the zinc ion has a possible effect on this bond distance. As discussed subsequently, the zinc ion has an apparent interaction with a nitrogen atom of the adjacent porphyrin ring.

The structures of the $[Ni(OEP^{\bullet/2})]_2^+$, $[Cu(OEP^{\bullet/2})]_2^+$, and $[Zn(OEP^{\bullet/2})H_2(OEP^{\bullet/2})]^+$ mixed-valence π-cation radicals in the solid state show that each forms a tight cofacial $\pi-\pi$ dimer. The interaction pattern for each of the derivatives is displayed in Figures 4 and 5, which give edge and top views. The pair of porphyrin rings in $[Ni(OEP^{\bullet/2})]_2SbCl_6$ are related by a 2-fold axis; the remaining two derivatives have porphyrin ring pairs related by an inversion center. Thus all three derivatives have a single crystallographically unique porphyrin ring. The two ring planes in the nickel derivative have a dihedral angle of 0.96°; the remaining two have dihedral angles of precisely 0° as required by the inversion symmetry. Table 4 gives a summary of the inter-ring geometry for all three derivatives. Tabulated are the Ct···Ct and M···M distances, the lateral shift of the two rings, and the mean plane separation. The relatively small values of the lateral shift are evident in Figure 5. The tight inter-ring interactions are also reflected in the orientation of the eight ethyl groups of each porphyrin ring; all ethyl groups are seen to point away from the center of the dimers.

(17) Sheldrick, G. M. *J. Appl. Crystallogr*. in preparation.

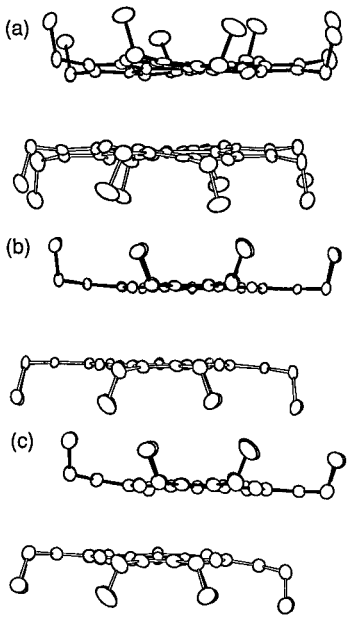

Figure 4. ORTEP diagrams showing edge-on-views of the cofacial $[Ni(OEP^{\bullet/2})]_2^+$, $[Cu(OEP^{\bullet/2})]_2^+$, and $[Zn(OEP^{\bullet/2})H_2(OEP^{\bullet/2})]^+$ mixed-valence π-cation radicals.

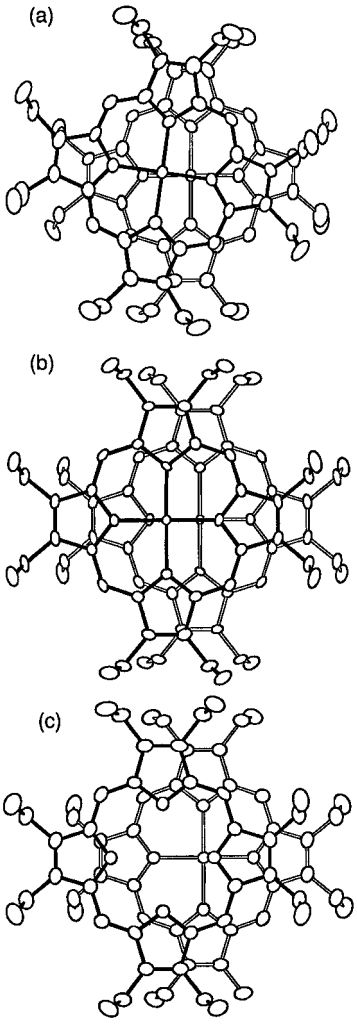

Figure 5. Top views of the $[Ni(OEP^{\bullet/2})]_2^+$, $[Cu(OEP^{\bullet/2})]_2^+$, and $[Zn(OEP^{\bullet/2})H_2(OEP^{\bullet/2})]^+$ mixed-valence π-cation radicals showing their lateral shifts.

Each mixed-valence cation is well-separated from the hexachloroantimonate anion in its respective crystal lattice. In all cases, the anion is well-behaved in the least-squares refinements despite the disorder involving the hexachloroantimonate anion and a lattice solvate molecule. ORTEP drawings of the hexachloroantimonate anion in the three structures are given in the Supporting Information.

Figure 6a is a formal diagram of the unique porphinato core in $[Ni(OEP^{\bullet/2})]_2^+$ showing the perpendicular displacement of each atom from the 24-atom mean plane. Also shown in the diagram are the average values of the distinct classes of bond distances and angles in the core of the derivative. The equivalent information for $[Cu(OEP^{\bullet/2})]_2^+$ is given in Figure 6b) and that for $[Zn(OEP^{\bullet/2})H_2(OEP^{\bullet/2})]^+$ in Figure 6c. The metal ion is displaced from the porphyrin core by the value given in Figure 6. In all cases, the metal atom displacement is toward the other ring of the binuclear monocation. The core conformations in the three derivatives are seen to be somewhat different. These differences appear to reflect the differing coordination requirements of the metal ion. The nickel derivative shows a modestly ruffled porphyrin core, while the other two species show modest C_{4v} doming of the porphyrin ring. In the latter two cases, the doming of the ring leads to closer interring separations at the ring center and larger separations at the ring periphery. A measure of the doming of the core can be given by noting the average displacement of various atom groups from the mean plane of the four nitrogen atoms: Cu, 0.03 Å; eight C_a's, −0.03 Å; four C_m's, −0.02 Å; eight C_b's, −0.08 Å. The analogous values for the zinc-containing complex are slightly larger.

Discussion

We report in this paper that the oxidation of neutral metallooctaethylporphyrin derivatives with 0.5 equiv of a one-electron oxidant leads to the preparation of a new class of crystalline, binuclear π-cation radical derivatives with the stoichiometry $[M(OEP^{\bullet/2})]_2SbCl_6$, rather than a reduced yield of a simpler oxidized product $[M(OEP^{\bullet})]SbCl_6$. Otherwise put, the reaction leads to new, oxidized species in which half of an electron per porphyrin ring is removed rather than the one full electron per porphyrin ring of "classical" π-cation radicals. This observation is perhaps surprising. However, the solid-state structures reported herein and the solution spectroscopic data reported elsewhere[14] make clear that these new mixed-valence π-cation radical complexes are stable and synthetically accessible, even in the absence of a stabilizing matrix or a specifically designed structure. The new complexes, which we call mixed-valence π-cation radicals, show some structural properties that are distinct from those of either the neutral or classical π-cation radicals.

All three complexes form dimers that have been illustrated in Figures 4 and 5. The interaction between the two porphyrin rings in these derivatives is of the $\pi-\pi$ type; there is no conventional covalent link joining the two rings. The interaction between two porphyrin rings can be described by the several parameters that have been tabulated in Table 4. These geometric parameters include the perpendicular separation between the two 24-atom cores, the lateral shift (or "slip") between the two rings, and the M···M and Ct···Ct distances.[12] These parameters are schematically depicted in Figure 7. It can be seen from Table 4 that the geometric parameters for the Ni and Cu homodimers are quite similar, while the Zn, H_2 heterodimer displays slightly larger separations. We believe that the differences in the heterodimer structure can be attributed to specific metal−porphyrin ring interactions that are absent in the other mixed-valence π-cation radical species. A comparison of the dimer structures of these derivatives with the interring interactions of other porphyrin systems is quite interesting.

Table 4. Crystallographic and Calculated Structural Parameters for $[Ni(OEP^{\bullet/2})]_2SbCl_6$, $[Cu(OEP^{\bullet/2})]_2SbCl_6$, and $Zn(OEP^{\bullet/2})H_2(OEP^{\bullet/2})]SbCl_6$

compound	$[Ni(OEP^{\bullet/2})]_2^+$	$[Cu(OEP^{\bullet/2})]_2^+$	$[Zn(OEP^{\bullet/2})H_2(OEP^{\bullet/2})]^+$
crystallographic relation of rings[a]	2-fold axis	inversion center	inversion center
interplanar angle, deg	0.96	0	0
metal atom displacement, Å[b]	0.04	0.07	0.19
mean plane separation, Å[c]	3.32	3.27	3.20
M···M distance, Å	3.434	3.375	3.228
Ct···Ct distance, Å[d]	3.514	3.502	3.547
lateral shift, Å	1.16	1.25	1.53
M−N_p distance, Å	1.950	1.984	2.053
slip angle, deg	19.4	21.0	25.6

[a] Symmetry operator relating the two porphyrin rings of the binuclear species. [b] Metal atom displacement from 24-atom core, positive displacement indicates metal atoms toward center of two rings. [c] The average mean plane separation for the two 24-atom cores of the dimer. [d] Ct is the center of a 24-atom porphyrin ring.

Table 5. Averaged Crystallographic and Calculated Structural Parameters for π-Cation Radical and Neutral Porphyrin Compounds[a]

compound	"classical" π-cation radical[b]	mixed-valence π-cation radical[b]	neutral class S[b]	neutral class I[b]
mean plane separation, Å[c]	3.25(6)	3.26(6)	3.42(8)	3.55(14)
Ct···Ct distance, Å[d]	3.26(6)	3.52(2)	3.79(15)	4.94(24)
lateral shift, Å	0.1(6)	1.31(19)	1.61(27)	3.48(47)
slip angle, deg	1.74(1.11)	22.0(3.2)	25.3(3.4)	43.8(3.6)

[a] Derivatives with alkyl substituents only. [b] Numbers in parentheses are calculated esd's that show dispersion in the total sample. [c] The average mean plane separation for the two 24-atom cores of the dimer. [d] Ct is the center of the 24-atom porphyrin ring.

Porphyrin systems commonly display inter-ring interactions in the solid state and in solution. Very strong porphyrin−porphyrin interactions are observed in the solid-state structures of four- and five-coordinate metallooctaethylporphyrin π-cation radical species.[9−11] There are now a total of eight different crystalline derivatives that have been structurally characterized; all are observed to form solid-state dimers. These π-cation radical dimers have virtually eclipsed porphyrin core pairs and rather small interplanar spacings; the similarity of the inter-ring structures is striking. The majority of neutral metalloporphyrins with nonaryl peripheral substituents have also been observed to form porphyrin−porphyrin dimers or higher aggregates in their solid-state structures. Scheidt and Lee[12] noted that these compounds had inter-ring interaction patterns that fell into three classes they called S, I, and W. Each class is distinguished by clustered ranges of geometric parameter values with significant gaps between classes. The lateral shift and slip angles are especially defining, while the interplanar spacings show somewhat larger variations. Classes S and I have structures consistent with inter-ring interactions stronger than those of class W, with class S showing stronger interactions than those of class I.

Values for the inter-ring interaction parameters of the π-cation radical species and the neutral porphyrin compound classes S and I are reported in Table 5; all represent interactions between unconstrained porphyrin ring pairs. The values shown for these three groups of structures suggest that the inter-ring geometry is dependent on the oxidation state of the porphyrin ring, with the π-cation radical species showing stronger inter-ring interactions. Values of the interplanar spacings and especially the lateral shifts and slip angles (which reflect the area of porphyrin ring overlap) are seen to vary in a monotonic fashion in the order π-cation radicals, class S and class I. If the inter-ring interactions are indeed responsive to the level of ring oxidation, then the mixed-valence π-cation species should have values that fall between those of class S and classical π-cation species. Indeed a comparison of values in Tables 4 and 5 reveals that this is precisely what is observed. Averaged values of interplanar spacings, lateral shifts and slip angles follow the order: π-cation radical < mixed-valence π-cation radical < neutral porphyrin (class S). We can thus conclude that the observed porphyrin inter-ring interactions are exquisitely sensitive to porphyrin ring oxidation level. The effect must surely derive from electronic interactions between the two rings; however, an analysis is beyond the scope of this paper. Such inter-ring specificity is the probable cause for two curious reports[18,19] concerning the oxidation of covalently linked diporphyrins. In these systems, some diporphyrins, but not all, undergo two stepwise one-electron oxidations, rather than a single two-electron oxidation. The remainder of the diporphyrin derivatives undergo a single two electron oxidation. It seems likely that the covalently linked diporphyrin systems that display single one-electron oxidation steps must be able to assume a structure that leads to delocalization of the radical electron over both porphyrin rings. The derivatives that cannot achieve such structures are likely to undergo oxidations in which both rings are oxidized simultaneously.

The crystal structures[6,7] of photosynthetic reaction centers show that the "special pair" consists of two associated bacteriochlorophyll molecules. The two bacteriochlorophyll rings are approximately parallel and show, within the limits of the structure determinations, the expected interplanar separation. The inter-ring overlap of the two bacteriochlorophylls is relatively small (i.e., the lateral shift is large) and shows some species variation. In the classification scheme of Scheidt and Lee,[12] the two rings are in the weakly interacting group W. Of course, the crystal structures of the photosynthetic reaction centers show the interaction geometry of two neutral bacteriochlorophyll rings. Our structural results for the neutral and mixed-valence π-cation radical derivatives show that the inter-ring geometry changes with ring oxidation level. This observation makes it tempting to suggest that the geometry of the special pair, P, would also change upon photooxidation to P^+. Such a structural change for the P to P^+ transition could provide a substantial barrier to the back reaction and contribute significantly to the extremely high quantum yield of the charge-separated state.

The structural parameters for the metal ions of the copper and nickel mixed-valence π-cation radical complexes are those expected for the neutral metallo complex with the same core conformation. The observed average Ni−N_p distance is 1.950(7) Å, marginally shorter than the distances observed in two planar forms of Ni(OEP)[20,21] but longer than the 1.929(3) Å

(18) Le Mest, Y.; L'Her, M.; Hendricks, N. H.; Kim, K.; Collman, J. P. *Inorg. Chem.* **1992**, *31*, 835.
(19) Osuka, A.; Nakajima, S.; Nagata, T.; Maruyama, K.; Toriumi, K. *Angew. Chem., Int. Ed. Engl.* **1991**, *30*, 582.
(20) Cullen, D. L.; Meyer, E. F., Jr. *J. Am. Chem. Soc.* **1974**, *96*, 2095.
(21) Brennan, T. D.; Scheidt, W. R.; Shelnutt, J. A. *J. Am. Chem. Soc.* **1988**, *110*, 3919.

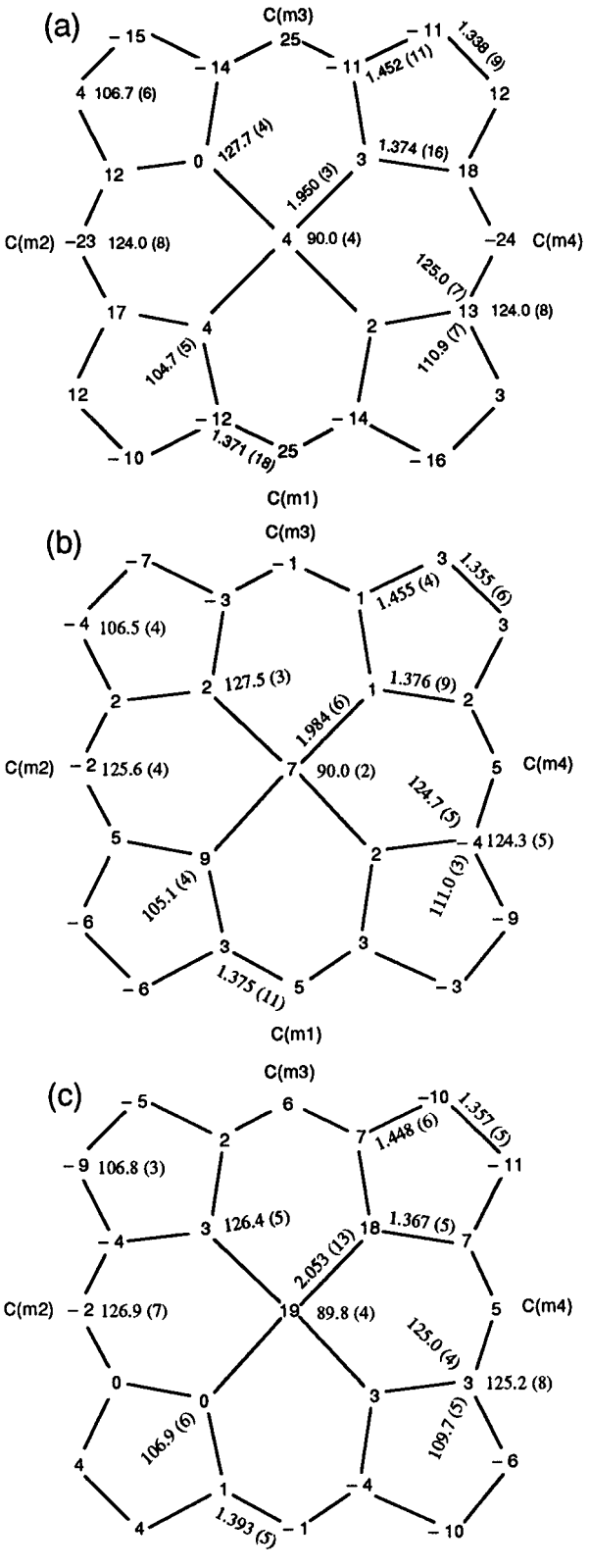

Figure 6. Formal diagram of the porphinato core in the $[Ni(OEP^{\bullet/2})]_2^+$, $[Cu(OEP^{\bullet/2})]_2^+$, and $[Zn(OEP^{\bullet/2})H_2(OEP^{\bullet/2})]^+$ molecules displaying the displacement, in units of 0.01 (Å), of each atom from the mean plane of the porphinato core.

value observed for the strongly S_4-ruffled conformational form of tetragonal Ni(OEP).[22] However, the degree of core distortion in $[Ni(OEP^{\bullet/2})]_2SbCl_6$ is significantly less than that of tetragonal Ni(OEP). A quantitative expectation for the Ni−N_p distance

(22) Meyer, E. F., Jr. *Acta Crystallogr., Sect. B* **1974**, *B28*, 2162.

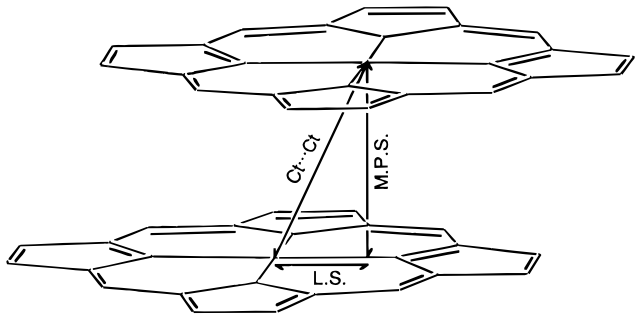

Figure 7. Diagram illustrating the geometric parameters used to describe dimers formed by two porphyrin rings.

in the complex with its less S_4-ruffled core can be made using the treatment suggested by Hoard;[23] the calculated value of 1.944 Å is within 1 standard deviation of the observed value.

The observed Cu−N_p bond distance in $[Cu(OEP^{\bullet/2})]_2SbCl_6$ is 1.984(6) Å, well within the range 1.971−2.010 Å observed for other copper porphyrinates.[24−26] In the copper derivatives, as in the nickel species, there are differences in the observed Cu−N_p distances that are related to core conformation. Nonplanar derivatives with D_{2d} core conformations (either ruffled or saddled) have Cu−N_p distances that are usually at the low end of the range, although the saddled species appear to display a wider range of metal ligand distances. Derivatives with planar cores typically display Cu−N_p distances of 2.00−2.01 Å. However, the porphinato core conformation in $[Cu(OEP^{\bullet/2})]_2SbCl_6$ is modestly "tented" (cf. Figure 6b). In this conformation, three of the pyrrole rings are tilted as in a C_{4v}-domed structure, while the fourth pyrrole ring forms the "open flap" of an umbrella tent. This type of core conformation does not appear to have an undue lengthening influence on the Cu−N_p bond distance, although such conformations are typically seen in metallo derivatives in which the metal ion size is moderately large in comparison to the central hole size of the porphyrin. This issue is of some significance in understanding the structure around the zinc ion in $[Zn(OEP^{\bullet/2})H_2(OEP^{\bullet/2})]SbCl_6$.

A description of the precise nature of the zinc mixed-valence system requires some elaboration. As we have noted earlier, the occupancy of zinc atoms in the binuclear system is only partial. This is the obvious result of (unplanned) partial demetalation of the starting material during the crystallization

(23) Hoard, J. L. *Ann. N.Y. Acad. Sci.* **1973**, *206*, 18.

(24) (a) Moustakali, I.; Tulinsky, A. *J. Am. Chem. Soc.* **1973**, *95*, 6811. (b) Song, H.; Reed, C. A.; Scheidt, W. R. *J. Am. Chem. Soc.* **1989**, *111*, 6865. (c) Pak, R.; Scheidt, W. R. *Acta Crystallogr., Sect. C* **1991**, *C47*, 431. (d) McGhee, E. M.; Godfrey, M. R.; Hoffman, B. M.; Ibers, J. A. *Inorg. Chem.* **1991**, *30*, 803. (e) Senge, M. O.; Smith, K. M. *Z. Naturforsch* **1993**, *48b*, 821. (f) Liddell, P. A.; Gerzevske, K. R.; Lin, J. J.; Olmstead, M. M.; Smith, K. M. *J. Org. Chem.* **1993**, *58*, 6681.

(25) (a) Fleischer, E. B.; Miller, C. K.; Webb, L. E. *J. Am. Chem. Soc.* **1964**, *86*, 2342. (b) Fuhrhop, J.-H.; Witte, L.; Sheldrick, W. S. *Liebigs Ann. Chem.* **1976**, 1537. (c) Sheldrick, W. S. *Acta Crystallogr., Sect. B* **1978**, *B34*, 663. (d) Collman, J. P.; Chong, A. O.; Jameson, G. B.; Oakley, R. T.; Rose, E.; Schmittou, E. R.; Ibers, J. A. *J. Am. Chem. Soc.* **1981**, *103*, 516. (e) Fillers, J. P.; Ravichandran, K. G.; Abdalmuhdi, I.; Tulinsky, A.; Chang, C. K. *J. Am. Chem. Soc.* **1986**, *108*, 417. (f) Woo, L. K.; Maurya, M. R.; Jacobson, R. A.; Yang, S.; Ringrose, S. L. *Inorg. Chem.* **1992**, *31*, 913. (g) Schaefer, W. P.; Hodge, J. A.; Hughes, M. E.; Gray, H. B. *Acta Crystallogr., Sect. C* **1993**, *C49*, 1342.

(26) (a) Erler, B. S.; Scholz, W. F.; Lee, Y. J.; Scheidt, W. R. *J. Am. Chem. Soc.* **1987**, *109*, 2644. (b) Nagata, T.; Osuka, A.; Maruyama, K. *Acta Crystallogr., Sect. C* **1990**, *C46*, 1745. (c) Henling, L. M.; Schaefer, W. P.; Hodge, J. A.; Hughes, M. E.; Gray, H. B. *Acta Crystallogr., Sect. C* **1993**, *C49*, 1743. (d) Renner, M. W.; Barkigia, K. M.; Zhang, Y.; Medforth, C. J.; Smith, K. M.; Fajer, J. *J. Am. Chem. Soc.* **1994**, *116*, 8582. (e) Kaufmann, T.; Shamsai, B.; Lu, R. S.; Bau, R.; Miskelly, G. M. *Inorg. Chem.* **1995**, *34*, 5073.

experiment. It has been shown[27] that oxidation of metalloporphyrins in CH_2Cl_2 often results in the formation of free base or porphyrin diacid impurities. The ease of demetalation is core size dependent, enhanced by trace amounts of acid; the easiest demetalation processes are those of the π-cation radicals of Mg or Zn. Finally, we note that the spectroscopic experiments described elsewhere[14] have shown that the heterobinuclear, zinc−free base mixed-valence π-cation radical species can be formed by an appropriate direct reaction.

The idealized formula ($[Zn(OEP^{\bullet/2})H_2(OEP^{\bullet/2})]SbCl_6$) requires a zinc occupancy factor of 0.5, but the least-squares refined value is slightly higher at 0.588(3). The mixed-valence π-cation radical site in all three mixed-valence structures is comprised of two porphyrin rings that are not crystallographically independent but are related by symmetry. The zinc system must be disordered, and the solid-state structure could contain three possible ring pairs identified by the central substituent: Zn−Zn, Zn−H_2, or H_2−H_2. The statistical population would be in the approximate ratio of 3:5:2. Observed structural features, as described below, suggest that the Zn−H_2 pair predominates beyond its statistically expected population; there would of course be decreases in the population of the other two possible pairs. The population of the Zn−H_2 pair could increase to a maximum of 80%.[28]

The core has a tented conformation (Figure 6c) similar to that in the copper system, but as we have already shown, this is not expected to significantly influence the geometry around the metal ion. The observed Zn−N_p bond distance in $[Zn(OEP^{\bullet/2})H_2(OEP^{\bullet/2})]SbCl_6$ is 2.053(13) Å, a bit larger than expected for four-coordinate species, which have Zn−N_p bond distances of ∼2.036 Å.[29] Rather, the observed Zn−N_p distance is at the low end of Zn−N_p distances seen for five-coordinate derivatives (range 2.051(3)−2.076(9) Å, average 2.067(9) Å).[30] Even more significant, however, is the out-of-plane displacement of the zinc ion (0.19 Å), which is toward the other ring of the dimer. The direction and magnitude of this displacement is much larger than expected for four-coordinate zinc complexes. The reason for the unexpectedly large zinc atom displacement is suggested when the structures of both rings of the binuclear complex are considered.

An unexpectedly large 0.18 Å displacement of pyrrole atom N(3) on the other porphyrin ring is toward the zinc atom and leads to an "axial" Zn−pyrrole nitrogen interaction. Although the "axial" Zn−N distance is 2.872 Å, this is substantially less than the interplanar spacing of 3.200 Å and is consistent with the idea that the pyrrole nitrogen atom is acting as a weak fifth ligand to zinc. A substantial tendency for zinc porphyrins to be five-coordinate is well-known,[31] and this tendency appears to be enhanced in π-cation radical dimer derivatives.[11,30b,f] The axial Zn−N interaction provides an additional component in the inter-ring interaction in the mixed-valence species. Such an interaction, which probably supplements the π−π interaction, also requires a larger value of the lateral shift than those observed in the two homonuclear dimers (cf. Table 4).

The unusual apparent conformation of the porphinato core with the large displacement of the N(3) atom of a planar pyrrole ring from the 24-atom mean porphyrin plane would seem more likely for an unmetalated porphyrin ring than a metallated ring.[32] We expect that the inter-ring structure of the Zn−Zn and the Zn−H_2 species would show some differences in the axial Zn−N(3) distance with the distance larger in the Zn−Zn derivative. We thus believe that the large distortions seen in $[Zn(OEP^{\bullet/2})H_2(OEP^{\bullet/2})]SbCl_6$ predominantly reflect the effects of an axial Zn−N(3) interaction in a heterobinuclear species. We note that the experimentally defined positions of the atoms are still the space average of at least two species and the axial Zn−N interaction is likely to be a bit tighter in pure $[Zn(OEP^{\bullet/2})H_2(OEP^{\bullet/2})]SbCl_6$ than that observed in the present disordered species.

Summary. The synthesis of three mixed-valence π-cation radical complexes, $[M(OEP^{\bullet/2})]_2^+$, M = Ni, Cu, and (Zn,H_2), are described. Molecular structure determinations show that all three species are cofacial binuclear complexes. Detailed ring−ring interactions appear to be exquisitely sensitive to the level of porphyrin ring oxidation. A comparison of structures suggests that there are characteristic dimeric geometries for noncovalently linked, cofacially dimeric neutral, mixed-valence π-cation radical and π-cation radical derivatives.

Acknowledgment. We thank the National Institutes of Health for support of this research under Grant GM-38401 (W.R.S.) and for the purchase of X-ray instrumentation under Grant RR-06709.

Supporting Information Available: Tables S1−S12 listing complete crystallographic details, atomic coordinates, anisotropic thermal parameters, and fixed hydrogen atom coordinates for $[Ni(OEP^{\bullet/2})]_2SbCl_6$, $[Cu(OEP^{\bullet/2})]_2SbCl_6$, and $[Zn(OEP^{\bullet/2})H_2(OEP^{\bullet/2})]SbCl_6$. Figures S1−S3 showing ORTEP plots of the $SbCl_6^-$ counterion in the three structures (22 pages). Ordering information is given on any current masthead page.

IC9610748

(27) Oertling, W. A.; Salehi, A.; Chang, C. K.; Babcock, G. T. *J. Phys. Chem.* **1987**, *91*, 3114.

(28) The population of the Zn−H_2 pair could increase to a maximum of 0.8, if all free base was paired with zinc.

(29) (a) Simonis, U.; Walker, F. A.; Lee, P. L.; Hanquet, B. J.; Meyerhoff, D. J.; Scheidt, W. R. *J. Am. Chem. Soc.* **1987**, *109*, 2659. (b) Scheidt, W. R.; Mondal, J. U.; Eigenbrot, C. W.; Adler, A.; Radonovich, L. J.; Hoard, J. L. *Inorg. Chem.* **1986**, *25*, 795. (c) Scheidt, W. R.; Kastner, M. E.; Hatano, K. *Inorg. Chem.* **1978**, *17*, 706.

(30) (a) Collins, D. M.; Hoard, J. L. *J. Am. Chem. Soc.* **1970**, *92*, 3761. (b) Spaulding, L. D.; Eller, P. G.; Bertrand, J. A.; Felton, R. H. *J. Am. Chem. Soc.* **1974**, *96*, 982. (c) Cullen, D. L.; Meyer, E. F. *Acta Crystallogr., Sect. B* **1976**, *B32*, 2259. (d) Hatano, K.; Kawasaki, K.; Munakata, S.; Litaka, Y. *Bull. Chem. Soc. Jpn.* **1987**, *60*, 1985. (e) Brennan, T. D.; Scheidt, W. R. *Acta Crystallogr., Sect. C* **1988**, *C44*, 478. (f) Song, H.; Rath, N. P.; Reed, C. A.; Scheidt, W. R. *Inorg. Chem.* **1989**, *28*, 1839. (g) Senge, M. O.; Eigenbrot, C. W.; Brennan, T. D.; Shusta, J.; Scheidt, W. R.; Smith, K. M. *Inorg. Chem.* **1993**, *32*, 3134.

(31) Hoard, J. L. In *Porphyrins and Metalloporphyrins*; Smith, K. M., Ed.; Elsevier Scientific Publishing Co.: New York, 1975; Chapter 8.

(32) Unless the metal ion is extremely large in comparison to the size of the central hole of the porphyrin, the four M−N_p interactions should lead to near 4-fold symmetry. Furthermore, a nonplanar distortion of a free base should be energetically more favorable than for a metalated species.